EVOLUTION
INTERNATIONAL JOURNAL OF ORGANIC EVOLUTION
SSE
SOCIETY for the STUDY of EVOLUTION

Evolution of cranial shape in a continental-scale evolutionary radiation of Australian lizards

Journal:	*Evolution*
Manuscript ID	19-0145.R1
Manuscript Type:	Original Article
Keywords:	Adaptive, Agamidae, Geometric morphometrics, Lizards, Phylomorphospace, Skull

Evolution of cranial shape in a continental-scale evolutionary radiation of Australian lizards

Abstract

Key words: adaptive, Agamidae, geometric morphometrics, lizards, phylomorphospace, skull

For adaptive radiations of animals, a defining character is a diversity of morphological forms that are associated with the use of different types of resources, following the invasion of vacant niches. The Australian agamid lizards (Amphibolurinae) exhibit a great deal of taxonomic, ecological and morphological diversity. However, there has not yet been an assessment of interspecific variation in their cranial morphology. Here, we use three-dimensional geometric morphometrics to characterise morphological diversity in the cranium of 52 species of Australian and Asian (sister group) dragon lizards, and investigate whether it matches patterns expected from the ecological process of adaptive radiation. Phylogenetic affinity, evolutionary allometry, and ecological life habit all play major roles in the evolution of cranial shape in the sampled dragon lizards. We find common themes of ecomorphology known from other lizard clades, where tree-dwelling species have long skulls and snouts, terrestrial species have short, blunt, robust crania, and saxicolous species have dorsoventrally shallow skulls. These characteristics likely result from trade-offs to optimise functional capabilities, which play a role in the evolution of cranial shape. It is likely that the continent of Australia presented the invading ancestral agamid with ecological opportunity, and environmental changes over the last 20Ma facilitated the radiation of lizards that may be considered adaptive.

Introduction

A key objective of evolutionary biology is to understand the processes underlying different patterns of morphological diversification. One such process, adaptive radiation, involves "the rapid evolution of morphologically and ecologically diverse species from a single ancestor" (Osborn 1902; Schluter 2000). A fundamental aspect of adaptive radiation is ecological opportunity, where certain conditions allow rapid speciation through adaptation to different niches (Losos and Mahler 2010). This speciation can result from factors such as new resources, freedom from competition, and an absence of predators and pathogens. Consequently, adaptive radiations are often linked to particular events, such as a clade invading a new geographic area or environment (Lovette et al. 2002), or following a major extinction event (Osborn 1902; Jarvis et al. 2014). For adaptive radiations of animals, one of their defining characters is a diversity of morphological forms that are functionally associated with the use of different types of resources following the invasion of a range of vacant niches (Cooper et al. 2010; Monteiro and Nogueira 2010; Dumont et al. 2011; Jønsson et al. 2012; Sanger et al. 2012; Wilson et al. 2012).

It has been hypothesised that island adaptive radiations represent a release from competition or a reduction in predation, and hence produce greater morphological and ecological diversity when compared to mainland radiations (Carlquist 1974; Losos and Ricklefs 2009). Australia is a distinctive case: although considered an island, because it is isolated and surrounded by sea, it is also a large continent. To explain the drivers behind Australian evolutionary radiations, it is important to consider the particular conditions that a clade's ancestor was presented with upon its arrival and subsequent diversification. There are two factors that highlight the potential for Australia to have presented an invading clade with ecological

opportunity (Schluter 2000). Firstly, up until 30 million years ago (Ma), Australia was likely deficient of almost all of the major squamate (lizards and snakes) clades (Oliver and Hugall 2017), which potentially provided squamate invaders with a release from competition. Secondly, around 20 Ma, Australia began to undergo aridification and reduction in rainforest cover (Fujioka et al. 2009; Fujioka and Chappell 2010), which potentially opened up empty niches for invaders. These environmental circumstances suggest that Australia would have presented arriving ancestors of Australian radiations with the ecological opportunities that would facilitate adaptive radiation.

Dated molecular phylogenies show that the deepest divergences of Australian arid-adapted squamate taxa evolved from mesic-adapted ancestors around the same time that aridification began (Keogh 1998; Ast 2001; Hugall et al. 2008; Sanders et al. 2008; Skinner et al. 2011; Vidal et al. 2012; Chen et al., 2013), and it is likely that these lineages were the result of oceanic dispersal from southern Asia (Oliver and Hugall 2017). Inferred palaeoclimate trends suggest an extensive warm mesic environment in Australia at around 25-16 Ma, followed by fragmentation via aridification from around 15 Ma, and inland desertification since 7 Ma (Fujioka et al. 2005; Fujioka et al. 2009; Fujioka and Chappell 2010). Rapid speciation within the arid zone is temporally consistent with the onset of aridification (Melville et al. 2001; Byrne et al. 2008; Shoo et al. 2008). Today, squamates make up the most taxonomically diverse constituent of the Australian vertebrate fauna and are distributed across the entire continent.

Amphibolurines are the Australian radiation of agamid lizards, and are a speciose (approximately 108 species) subfamily, making up approximately 20% of all Australian squamates, with a relatively well-resolved phylogeny (Hugall et al. 2008; Melville et al. 2011; Pyron et al. 2013). They comprise four distinct groups (Figure 1). First the taxa that are least

nested (cf. Sereno 1999), herein referred to as the "LN group", branched off outside the major furcation of the amphibolurine clade and includes a handful of rainforest adapted and semi-aquatic species, as well as the iconic thorny devil, *Moloch horridus* (Hugall et al. 2008). The second clade, comprises *Intellagama* plus a monophyletic grouping of the remaining amphibolurine species. This diverse clade is divided into two further clades that make up the core of the amphibolurine radiation: the *"Ctenophorus* group" and the "*Amphibolurus* group" (of Hugall et al. 2008). The *Ctenophorus* group is comprised of a single speciose genus (29 species), found throughout most of Australia and comprised of predominantly small, terrestrial dragons. The *Amphibolurus* group comprises ten genera and, includes both semi-arboreal and terrestrial dragons. Generic diversity ranges from genera that contain a single species (e.g. *Rankinia*), to the much more speciose *Diporiphora* (22 species).

Amphibolurines are ecologically diverse and have adapted to life on and off the ground, inhabiting burrows, soil, grass, rocks, stumps, shrubs, and trees (Pianka and Pianka 1970; Pianka 1971; Collar et al. 2010; Pianka 2013c, b, a, 2014) (see Figure 1). They have also developed many strategies for evading predators and catching prey, including speed (Cogger 2014), crypsis (Shoo et al. 2008), defensive displays (Throckmorton et al. 1985; Shine 1990), and spines (Pianka and Pianka 1970). They exhibit great variation in their skull anatomy (e.g. Siebenrock 1895; Bell et al. 2009; Gray et al. 2017, Gray et al. 2019; Stilson et al. 2017). However, detailed interspecific examination of variation in amphibolurine cranial morphology in an ecological context has yet to be attempted. They are considered to be an ecologically and evolutionarily successful group, phylogenetic work has shown that their radiation was relatively rapid, and post-dates the Oligocene (Chen et al. 2012). However, their potential to be defined as an "adaptive radiation" has not yet been explicitly investigated.

The main aim of this paper is to characterise the morphological diversity in the amphibolurines, and investigate whether it matches patterns expected from the ecological process of adaptive radiation (Ricklefs 2004; Gavrilets and Losos 2009). We use three-dimensional geometric morphometrics to characterise cranial shape in a dataset of 52 species of agamid lizards, representing the broad range of phylogenetic and morphological diversity of Australian agamid lizards and their Asian sister clade (Draconinae). Skull morphology is a good indicator of ecological diversity in lizards (e.g. Stayton 2004; Hipsley and Müller 2017) and thus a useful model for studies of adaptive evolution. In an adaptive radiation, ecological factors play a key role in evolution, and therefore skull morphology should be significantly linked to adaptive ecology and ecological groups should be found in association in morphospace (Clabaut et al. 2007). We map the current phylogenetic hypothesis into the morphospace to infer aspects of the evolutionary history of cranial shape, using the phylomorphospace approach (sensu Sidlauskas 2008). We perform statistical analyses that enable us to assess the adaptive character of this radiation of lizards, and consider the potential for particular skull shapes to be beneficial for adapting to different ecological zones.

Material and methods

Study samples

We sampled 52 individuals representing 52 species from the lizard family Agamidae: 44 from the Australian clade, Amphibolurinae, and eight from its Asian sister clade, Draconinae. Specimens which included both intact, alcohol preserved specimens and dry skeletal skull specimens were sampled primarily from the herpetology collection at South Australian Museum,

Adelaide, and the Australian Museum in Sydney (see Appendix 1: Table S1, for specimen information). Sampling included at least one representative from each currently recognised amphibolurine genus except *Cryptagama*. Closely related Draconinae species (sister group to the Australian radiation) were included to expand morphological and ecological sampling. All specimens were adults, as identified by a complete acrodont tooth row (Cooper et al. 1970).

Phylogeny

To infer the phylogenetic tree (Fig. 1) we used a combination of the most recent relevant phylogenetic studies (Melville et al. 2001; Hugall et al. 2008; Shoo et al. 2008; Melville et al. 2011; Pyron et al. 2013; Melville et al. 2014). We built a topological synthesis (i.e. without branch lengths) of well supported phylogenetic relationships using Mesquite v 3.51 (Maddison and Maddison 2018). Branch lengths were subsequently estimated using the *ape* R package (Popescu et al. 2012) function "compute.brlen", which uses the Grafen (1989) computation method. We defined and examined five major monophyletic clades in our data set: the Draconinae; the least nested (LN) group; *Intellagama*; the *Amphibolurus* group; and the *Ctenophorus* group.

Ecological categories

Life habit categorisations for species are based in information available in Wilson and Swan (2013), Cogger (2014), Grismer (2011), Kaiser et al. (2011), Somaweera and Somaweera (2009), and Jansen and Bopage (2011):

Arboreal: Primarily observed in trees and rarely on the ground.

Semi-arboreal: Observed spending considerable time on the ground and in trees or shrubs.

Terrestrial: Primarily observed on the ground, may use or dig burrows.

Saxicolous: Primarily confined to rocky ranges and outcrops.

X-ray computed tomography

To obtain digital reconstructions of skulls for measurement, we used high resolution X-ray micro computed tomography (CT) on the heads of whole specimens preserved in alcohol, and skeletal skull specimens. All CT scans were made with the Skyscan 1076 system at Adelaide Microscopy, at the University of Adelaide. Specimens were scanned with a voxel size of either 8 or 16 microns, dependent on the size of the specimen, with an appropriate range of X-ray settings including a current range of 100-250 μA, and a voltage range of 36-82 kV. An aluminium (0.5 mm) filter was used for all scans. CT scan data was reconstructed using Bruker Nrecon software v 6.6.9.4 (Skyscan 2011). 3D volumes were processed using Avizo v 9.0 (Visualization Sciences Group 2013): bone was digitally segmented by applying a threshold that generated the full three-dimensional anatomy of the skull without obscuring details such as suture seams. We removed associated elements (lower jaws, hyoids, scleral ossicles, and vertebrae), and converted the cranium to a 3D surface model (a triangular mesh of approximately one million faces).

Landmarking and shape analysis

To characterise cranial shape, we used 3D landmark-based geometric morphometric methods (Bookstein 1996; Dryden and Mardia 1998; Klingenberg 2010; Gray et al. 2017). We digitised 102 landmarks in 3D over each cranium model (Fig. 2, see also Appendix 2: Table S2, for landmark definitions), which represented the cranial shape and were placed at equivalent points on bones at sutures, and extremes and boundaries of curvature of major structures, using Landmark Editor v 3.0.6 (Wiley et al. 2007). To confirm that our landmark set was sufficient to

capture the shape variation in our sampled species, we used the "lasec" function in the R package *laMBDA* v 1.0.9 (Watanabe 2018) (landmark sampling curve in Appendix 3: Fig. S1). Landmark data were subjected to generalised Procrustes alignment (GPA) and projection into tangent space using the R package *geomorph* v 3.0.6 (Adams et al. 2018). The Procrustes fit corrected for object asymmetry, and we extracted coordinates for the symmetric component of shape (Klingenberg et al. 2002). These Procrustes-aligned coordinates were used in subsequent analyses. All analyses were performed in the R statistical environment v 3.5 (R Core Team 2018) and functions refer to the *geomorph* package unless otherwise stated.

Effect of phylogeny, evolutionary allometry, and life habit on skull shape

To assess the degree to which variation in cranial shape among the sampled agamid species is evolutionarily associated with size variation (evolutionary allometry, see Klingenberg 1996) and ecology, we performed a phylogenetic generalised least-squares (PGLS) analysis of shape on log-transformed size and life habit while accounting for the phylogenetic relationships among agamid species, using the "procD.pgls" function. The "procD.pgls" function performed 1000 permutations of shape data across the tips of the tree, and estimates were compared to observed values to assess significance (Adams and Collyer 2018). Centroid size (a measure of size extracted from the landmarks (Dryden and Mardia 1998); was used to represent head size. To visualise evolutionary allometry, we carried out a multivariate regression and calculated the regression score (Drake and Klingenberg 2008) using "procD.allometry" function, and plotted this against size with the points identified by life habit and phylogenetic group. To illustrate the shape differences associated with the minimum and maximum skull sizes, we used to "plotRefToTarget" function to warp a mesh representing the mean specimen to shapes representing the predicted shapes at the smallest and largest centroid size in the data set.

We used allometry-free skull shape variables to examine the shape variation not associated with evolutionary allometry. To obtain allometry-free shape variables, we used a multivariate adaptation of phylogenetic size correction methods (Klingenberg 2016). To obtain allometry-free shape variables for each specimen, we performed a regression of shape on size using "procD.pgls", which computed the regression residuals for the cranial shape of each species, and these were added to the original shape variables. To examine phylogenetic structure in the cranial morphospace, we performed a principal component analysis (PCA) and generated a cranial morphospace by plotting the main axes of shape variation (see Appendix 4: Fig. S2 for PCA before allometry was corrected for). We projected the phylogeny into the cranial morphospace by estimating ancestral states of the internal nodes by maximum likelihood, using the "phylomorphospace" function in the R package *phytools* (Revell 2012). To evaluate the degree of phylogenetic signal present in the shape and size variables relative to expectations under a Brownian motion model of evolution, we used the "physignal" function in *geomorph*, which uses K_{mult}, a mathematical generalisation of the K statistic (Blomberg et al. 2003) for highly multivariate data (Adams 2014). Significance was tested for by 1000 permutations of data among the tips of the phylogenetic tree.

We quantified the amount of convergence in cranium shape using a morphospace distance-based approach (Stayton 2015a). This method is based on the idea that convergence occurs when two taxa evolve to be more similar than their estimated ancestors were to one another (Losos 2011; Stayton 2015b), and produces an index of convergence. For sampled agamid crania, we calculated the index of convergence for each ecological life habit group in a morphospace defined by PCs 1-4. We used the "convrat" function in the R package *convevol* v 1.3 (Stayton 2015b), which quantifies convergent evolution by inferring ancestral states using

weighted means of extant species data and scaling the convergence index to permit comparison among different taxa. We used the function "convratsig" to test for significance of each convergence estimate, which compares the observed distances to 1000 simulated dataset under a Brownian motion model of evolution.

To compare morphological disparity between the two most speciose clades of the Amphibolurinae, the *Ctenophorus* group and the *Amphibolurus* group (sister clades that effectively represent the core of the Australian radiation) we used the "morphol.disparity". This function calculates the Procrustes variance of each group, using residuals of a linear model fit (Zelditch et al. 2012). Significance was evaluated by 1000 permutations, where vectors of residuals were randomised among the two groups. To visualise these differences in the cranial morphospace, we used convex hulls to represent Procrustes variance.

To observe and describe the shape differences associated with the main axes of variation in the allometry-free shape variables, we used to "plotRefToTarget" function to warp a mesh representing the mean shape using the thin-plate spline approach to shapes representing the minimum and maximum values for the first four principal components (PCs).

Results

Skull shape is significantly associated with both size and life habit. A PGLS model evaluating the influence of cranial size and ecology on cranial shape (see Table 1) revealed that 11% of the total variance of shape is significantly associated with size variation (***P* = 0.001**), and 14% of the total variance of shape is significantly associated with life habit (***P* = 0.001**). Life habit categories were mostly partitioned along the allometric trajectory (Fig. 3A). Greater cranium size is associated with: a longer and dorsoventrally shallower snout; broader and more robust postorbitals and temporal bars (jugals, postorbits); larger and longer supratemporal

fenestra; smaller orbits; dorsoventrally straighter tooth rows; a broader anterior end to the frontal; and a more anteriorly located braincase (see Fig. 3B). Smaller cranium size is associated with: a shorter and more rounded snout; more slender and narrower postorbitals and temporal bars; smaller and shorter upper temporal fenestra; larger orbits; more dorsoventrally curved tooth rows; a narrower anterior end to the frontal; and a more posteriorly located braincase (see Fig. 3B).

The PCA of allometry-free shape variables revealed that most (57.74 %) of the shape variation among species is concentrated in four dimensions (out of 52, see Appendix 5: Table S3 for summary of first six PCs) with subsequent PCs each contributing only small amounts (<5%). PC1 describes 33.33% of the total shape variation. Low PC1 scores represent a relatively long, narrow, and posteriorly rounded skull with a rounded orbit, whereas high PC1 scores represent a relatively short, wide, and posteriorly angular skull with a dorsoventrally compressed orbit (Figure 4). This axis also describes differences between a dorsoventrally straight tooth row (high values), and one that curves dorsally at its anterior end (low values). PC2 describes 11.66% of the total variation. Low PC2 scores represent a dorsoventrally shallow and elongate skull whereas high PC2 scores represent a short, dorsoventrally deep skull with an extremely blunt snout (Figure 4). PC3 (7.20%) mainly describes differences between *Tympanocryptis* and other species and the rest of the sample. Low PC3 scores represent a shorter but more pointed snout and robust "cheek" (in lateral view the postorbital bar comprised of the jugal) whereas high PC3 scores represent a longer but more rounded snout and more gracile jugal. PC4 (5.55%) mostly describes differences in the relative length of the frontal. Low PC4 scores represent skulls with a shorter and wide frontal whereas high PC4 scores represent skulls with a long and narrow frontal. It also describes relative changes in the arrangement of the postorbit, jugal, and

248 squamosal bones, with the junction between the external suture seams located lower in lateral
249 view associated with lower PC4 scores. The maxilla varies from more slender at minimum
250 values to broader and more robust at maximum values.

251 Tests for phylogenetic signal (relative to what is expected under a Brownian motion
252 model of evolution) revealed that, while significant, the amount of signal is very low in both
253 cranial shape and size of the sampled agamid lizards (shape: $\boldsymbol{P = 0.001}$, $K_{mult} = 0.112$; size: $\boldsymbol{P =}$
254 $\mathbf{0.001}$, $K_{mult} = 0.1786$). These results, and the many crisscrossing branches in the
255 phylomorphospace (see Fig. 5) suggest that there is substantial homoplasy in cranial shape of the
256 sampled agamids. The four ecological life habit categories used in this study were associated
257 with particular areas of the cranial morphospaces (Fig. 5). Arboreal species occupy an almost
258 exclusive area of PC1 versus PC2 morphospace (Fig. 5A) representing low PC1 values (deep
259 narrow skull). Semi-arboreal species are relatively disparate but generally have low PC1 and
260 PC2 scores (long snout, narrow skull), and overlap with terrestrial and saxicolous species of
261 dragons. Terrestrial species largely overlap with semi-arboreal species, but also extend into their
262 own area of morphospace, associated with high PC1 values and low PC2 values (blunt snout,
263 wide skull). Saxicolous species overlap a little with semi-arboreal and terrestrial species, but
264 mostly occupy their own area of the morphospace, associated with high PC1 values and low PC2
265 values (dorsoventrally shallow skulls, Fig. 5A). Saxicolous species occupy a small area of the
266 PC3 versus PC4 morphospace (Fig. 5B), with average PC3 and PC4 values. Semi-arboreal and
267 arboreal species exhibit a very similar distribution, covering the entire range of PC4 values, with
268 average PC3 values. Terrestrial species cover the entire range of PC3 values, and (excluding
269 *Moloch*) exhibit high PC4 values.

Convergence index (C_1) values indicate that dragons belonging to the same ecological life habit groups have evolved to be more similar to each other than would be expected under a null model of Brownian motion evolution (arboreal $C_1 = 0.164$, $P = 0.12$; semi-arboreal $C_1 = 0.141$, $P = 0.066$; terrestrial $C_1 = 0.155$, $P = 0.137$; saxicolous $C_1 = 0.218$, $\mathbf{P = 0.016}$).

While there is no clear association between clade affiliation and evolutionary allometry (see Fig. 3A), members of the same clade seem to be associated with one another in the allometry-free cranial morphospace (Fig. 6). Draconines and the LN group (apart from *M. horridus*), mostly exhibit low PC1 values and high PC2 values, but are separate from each other within this area, with the LN group having lower PC1 values. The core of the amphibolurine radiation (*Ctenophorus* group and *Amphibolurus* group) occupy the opposite side of the PC1 versus PC2 morphospace, and the two groups overlap substantially with one another (Fig. 6A). Draconines exhibit a narrow range of relatively average PC3 values, while the LN group are spread over high PC3 values. The *Amphibolurus* groups and the *Ctenophorus* group overlap substantially along PC3, however the *Ctenophorus* group extend their range into high PC3 values, while the *Amphibolurus* group extend their range into low PC3 values. Members of Draconinae and the LN group are spread along PC4. The *Ctenophorus* group and the *Amphibolurus* group overlap substantially along PC, but the *Amphibolurus* group extend their range into low values of PC4. The morphological disparities of the *Amphibolurus* group (Procrustes variance = 0.00538) and the *Ctenophorus* group (Procrustes variance = 0.00515) are not significantly different from one another ($P = 0.856$) (Fig. 5). Despite some overlap along PCs 1-4, both groups also expand into their own exclusive areas of the cranial morphospaces. PC1 is thus related to major differences between draconines and amphibolurines, and PC2 is related to difference between *Moloch*, and the rest of the sample.

Discussion

Australia, with its vast array of different habitats and biomes, is an ideal place in which to explore the drivers of evolutionary radiation. We set out to do this using the Australian radiation of agamid lizards. Broadly, an adaptive radiation is the evolution of ecological and phenotypic diversity in a rapidly multiplying lineage (Schluter 2000). According to Schluter (2000), descendant species fit the "adaptive" criteria if there is an association between diverse phenotypes and their divergent environments. We explored the phenotypic variation in crania of Australian radiation of agamid lizards, and revealed that ancestral amphibolurines gave rise to new clades that today exhibit a morphologically-diverse array of skull shapes. However, the pattern of morphological variation within the sampled agamid skulls is not closely tied to phylogenetic relatedness. Instead, species with the same life habits share morphological features and occur in association in the cranial morphospace, even when they are not each other's closest relatives. This emphasises the adaptive character of these lizards, and suggests they are strong contender to be considered an "adaptive radiation".

There is surprisingly little phylogenetic signal in skull shape among the sampled agamids. A lack of distinct phylogenetic structure is evident from the criss-crossing patterns of branches within amphibolurine genera, and extensive overlap of branches within the cranial morphospace, and this pattern has also been observed to occur in juvenile amphibolurine species (Gray et al. 2019). These patterns indicate that morphological similarity is not solely due to phylogenetic relatedness. The range of potential skull shapes seems to be limited to a particular region of morphospace, but within this space, evolution is relatively free and labile. This pattern is similar

to that observed in species of bird (Tokita et al. 2017), mammal (Goswami et al. 2014), and fish (Clabaut et al. 2007). To describe a similar pattern, Goswami et al. (2014) used the analogy of a fly trapped within a tube. We suggest evolution of the sampled agamid lizards is more analogous to a fly in a deflated balloon, as there seems to be some flexibility around the peripheral areas of the occupied morphospace. This flexibility allows the evolution of more extreme skull shapes for particular ecological groups, e.g. the very dorsoventrally shallow skulls of rock dwellers, and the particularly blunt-faced skulls of some terrestrial species (that also happen to be burrowers: see Cogger, 2014). The patterns we observe in the cranial morphospace suggest that multiple cases of convergent and parallel evolution, and rapid morphological diversification exist in the Australian agamid lizard clade, and deserve further attention. Results suggest that there has been natural selection for similar skull shapes within life habit groups, and that a saxicolous lifestyle facilitates convergence on a particularly dorsoventrally shallow cranium. Even though tests for convergence did not produce significant results for the other life habit groups, this does mean ecological habit groups have not evolved to fill in a previously unoccupied region of morphospace that is suited to a particular life habit (e.g. Friedman 2009). It might be that their capacity to rapidly evolve a variety of different phenotypes may have led to a greater potential to exploit their respective environments (Vermeij 1973).

If shared evolutionary history is not the main factor influencing similarities in the skull shapes among amphibolurine lizards, then the convergent evolution we observe in this clade is probably the result of comparable ecological conditions (Sturmbauer et al. 2003). Australian agamid skulls are distributed in the morphospace according to their life habit, and statistical tests confirmed that particular skull shapes are similar because of shared ecological characteristics. Our study adds to the growing body of literature showing that ecological role frequently

338 overrides phylogenetic inheritance on a macroevolutionary scale (Clabaut et al. 2007; Pierce et
339 al. 2008; Kimmel et al. 2009; Stayton 2011; Sakamoto and Ruta 2012; Casanovas-Vilar and van
340 Dam 2013; Hipsley and Müller 2017). It seems clear that ecological opportunity can be a
341 powerful driver of morphological diversification, but it is also increasingly apparent that the
342 morphological variation in any given clade is a consequence of the combination and interaction
343 of several factors. Allometry, phylogeny, ecology, and development are all factors that determine
344 morphological diversity, but which factors have the greatest influence over morphological
345 variation, and to what extent, differs amongst clades.

346 The strong association between distribution of species in the cranial morphospace and
347 ecological life habit indicates divergent selection for agamid lizards with different ecological life
348 habits. Since selection acts, not directly on phenotypes, but on the functional capabilities of those
349 phenotypes (Arnold 1983; Garland and Losos 1994) it is likely that homoplastic aspects of skull
350 shape represent important functional aspects for life habit strategies. For example, the length of
351 the snout has an effect on the length of the out-lever, and consequently, an effect on bite force
352 (Olson 1961, Jones 2008, Lappin and Jones 2014). Although an elongate snout is therefore
353 associated with a reduced anterior bite force, there is also evidence that longer snouts can
354 enhance capture efficiency of highly mobile prey (Kohlsdorf et al. 2008). Furthermore, having a
355 dorsoventrally deeper head may involve a further trade-off between greater bite forces (more
356 space for jaw muscles), and faster climbing speeds (shallow heads keep the centre of mass is
357 closer to the substrate) (Herrel et al. 1999; Herrel et al. 2001). Our results indicate that ecological
358 trade-offs may be operating to optimise function in different habitats, and is a major factor that
359 has shaped the evolution of skull shape in Australia's agamid lizard radiation.

Our study brings the adaptive character of amphibolurine lizards to light, even though specific interpretations are difficult, with various ecological parameters acting concurrently on the evolution of skull shape. In reality, life habit for these lizards may be considered a continuum, with various species displaying different extents of their assigned category. Our categories are a simplification of life history but this issue reflects the problem of characterising animals that live in complex environments for which field data remains lacking. This system would benefit from an in-depth ecological assessment akin to the perch height and diameter information of Caribbean lizard habitats (Losos 1990). A more detailed examination of the relationship between life history and skull shape may be possible in the future following further field research. There remains a lot to be gained from studying this system in more detail, including more in-depth ecological assessments, and exploratory investigation of the anatomy and function underlying the different skull shapes characterised here. Furthermore, similar work investigating the morphological diversification of other Australian squamate clades that are estimated to have arrived around a similar time would broaden our understanding of whether environmental change on the large, squamate-poor, island continent of Australia, may have facilitated adaptive radiation.

Conclusions

Our study uncovered the major patterns of morphological variation in amphibolurine lizards, and revealed that the constraint of shared ancestry (as estimated by our phylogeny) on the Australian radiation of agamid lizards is low. Instead, a broad array of different skull shapes exist associated with ecological life habit, as expected for an “adaptive radiation” (Schluter 2000). The major patterns of variation involve orbital size, snout shape and length, skull depth, and size and robustness of postorbit elements: aspects of the skull related to jaw arrangement muscle size and

jaw outlever. We suggest that a combination of evolutionary lability and ecological opportunity, presented to the ancestral agamid upon its arrival to Australia, and subsequent environmental changes, has culminated in a radiation of lizards that may indeed be considered “adaptive”.

References

Adams, D. C. 2014. A generalized K statistic for estimating phylogenetic signal from shape and other high dimensional multivariate data. Syst Biol 63:685-697.

Adams, D. C. and M. L. Collyer. 2018. Multivariate phylogenetic comparative methods: evaluations, comparisons, and recommendations. Syst Biol 67:14-31.

Adams, D. C., M. L. Collyer, and Kaliontzopoulou. 2018. geomorph: software for geometric morphometric analyses. R package version 3.0.6. https://CRAN.R-project.org/package=geomorph.

Arnold, S. J. 1983. Morphology, performance and fitness. Amer Zool 23:347-361.

Ast, J.C. 2001. Mitochondrial DNA evidence and evolution in Varanoidea (Squamata). Cladistics 17:211-226.

Blomberg, S. P., T. J. Garland, and A. R. Ives. 2003. Testing for phylogenetic signal in comparative data: behavioural traits are more labile. Evolution 57:717-745.

Bookstein, F. L. 1996. Biometrics, biomathematics and the morphometric synthesis. Bull Math Biol 58:313.

Byrne, M., D. K. Yeates, L. Joseph, M. Kearney, J. Bowler, M. A. J. Williams, S. Cooper, S. C. Donnellan, J. S. Keogh, R. Leys, J. Melville, D. J. Murphy, N. Porch, and K. H. Wyrwoll. 2008. Birth of a biome: insights into the assembly and maintenance of the Australian arid zone biota. Mol Ecol 17:4398-4417.

Carlquist, S. 1974. Island biology. Columbia University Press, New York & London.

Casanovas-Vilar, I. and J. van Dam. 2013. Conservatism and adaptability during squirrel radiation: what is mandible shape telling us? PLOS ONE 8:e61298.

Chen, I-P., Symonds, M.R.E., Melville, .J, Stuart-Fox, D. 2013. Factors shaping the evolution of colour patterns in Australian agamid lizards (Agamidae): a comparative study. Biol J Linnean Soc 109:101-112.

Clabaut, C., P. M. E. Bunje, W. Salzburger, and A. Meyer. 2007. Geometric morphometric analyses provide evidence for the adaptive character of the tanganyikan cichlid fish radiations. Evolution 61:560-578.

Cogger, H. 2014. Reptiles and amphibians of Australia. CSIRO Publishing, Collingwood.

Collar, D. C., J. A. Schulte, B. C. O’Meara, and J. B. Losos. 2010. Habitat use affects morphological diversification in dragon lizards. J. Evol. Biol. 23:1033-1049.

Cooper, J. S., D. F. G. Poole, and R. Lawson. 1970. The dentition of agamid lizards with special reference to tooth replacement. J Zool 162:85-98.

Cooper, W. J., K. Parsons, A. McIntyre, B. Kern, A. McGee-Moore, and R. C. Albertson. 2010. Bentho-pelagic divergence of cichlid feeding architecture was prodigious and consistent during multiple adaptive radiations within African rift-lakes. PLOS ONE 5:e9551.

Drake, A. G. and C. P. Klingenberg. 2008. The pace of morphological change: historical transformation of skull shape in St Bernard dogs. Proc R Soc B 275:71-76.

Dryden, I. and K. Mardia. 1998. Statistical shape analysis, John Wiley & Sons.

Dumont, E. R., L. M. Dávalos, A. Goldberg, S. E. Santana, K. Rex, and C. C. Voigt. 2011. Morphological innovation, diversification and invasion of a new adaptive zone. Proc R Soc B 279:1797-1805.

Friedman, M. 2010. Explosive morphological diversification of spiny-finned teleost fishes in the aftermath of the end-Cretaceous extinction. Proc R Soc B 277:1675-1683.

Fujioka, T. and J. Chappell. 2010. History of Australian aridity: chronology in the evolution of arid landscapes. Geol. Soc., Special Publications 346:121-139.

Fujioka, T., J. Chappell, L. K. Fifield, and E. J. Rhodes. 2009. Australian desert dune fields initiated with Pliocene–Pleistocene global climatic shift. Geology 37:51-54.

Fujioka, T., J. Chappell, M. Honda, I. Yatsevich, L. K. Fifield, and D. Fabel. 2005. Global cooling initiated stony deserts in central Australia 2–4 Ma, dated by cosmogenic 21Ne-10Be. Geology 33:993-996.

Garland, T. J. and J. B. Losos. 1994. Ecological morphology of locomotor performance in squamate reptiles. Pp. 240-302 *in* P. C. Wainwright, and S. M. Reilly, eds. Ecological morphology: integrative organismal biology. The University of Chicago Press, Chicago & London.

Gavrilets, S. and J. B. Losos. 2009. Adaptive radiation: contrasting theory with data. Science 323:732-737.

Goswami, A., J. B. Smaers, C. Soligo, and P. D. Polly. 2014. The macroevolutionary consequences of phenotypic integration: from development to deep time. Phil Trans R Soc B 369:20130254.

Grafen, A. 1989. The phylogenetic regression. Phil Trans R Soc B 326:119-157.

Gray, J. A., McDowell, M. C., Hutchinson, M. N., Jones, M. E. H. 2017. Geometric morphometrics provides an alternative approach for interpreting the affinity of fossil jaws. J Herpetol 51:375-382

Gray, J. A., Sherratt, E., Hutchinson, M. N., Jones, M. E. H. 2019a. Changes on ontogenetic patterns facilitate diversification in skull shape of Australian agamid lizards. BMC Evol Biol 19:7

Gray, J. A., Hutchinson, M. N., Jones, M. E. H. 2019b. Exceptional disparity in Australian agamid lizards is a possible result of arrival into vacant niche. Anat Rec DOI:10.1002/ar.24096.

Grismer, L. L. 2011. Lizards of Peninsular Malaysia, Singapore and their adjacent archipelagos. Edition Chaimera, Germany.

Herrel, A., P. Aerts, J. Fret, and F. de Vree. 1999. Morphology of the feeding system in agamid lizards: ecological correlates. Anat Rec 254:496-507.

Herrel, A., R. V. Damme, B. Vanhooydonck, and F. D. Vree. 2001. The implications of bite performance for diet in two species of lacertid lizards. Can J Zoology 79:662-670.

Hipsley, C. A. and J. Müller. 2017. Developmental dynamics of ecomorphological convergence in a transcontinental lizard radiation. Evolution 71:936-948.

Hugall, A. F., R. Foster, M. Hutchinson, and M. S. Y. Lee. 2008. Phylogeny of Australian agamid lizards based on nuclear and mitchondrial genes: implications for morphological evolution and biogeography. Biol. J. Linnean Soc. 93:343-358.

Jansen, P. and M. Bopage. 2011. The herpetofauna of a small and unprotected patch of tropical rainforest in Morningside, Sri Lanka. Amphib Reptile Conserv 5:1-13.

Jarvis, E. D., S. Mirarab, A. J. Aberer, B. Li, P. Houde, C. Li, S. Y. W. Ho, B. C. Faircloth, B. Nabholz, J. T. Howard, A. Suh, C. C. Weber, R. R. da Fonseca, J. Li, F. Zhang, H. Li, L. Zhou, N. Narula, L. Liu, G. Ganapathy, B. Boussau, M. S. Bayzid, V. Zavidovych, S. Subramanian, T. Gabaldón, S. Capella-Gutiérrez, J. Huerta-Cepas, B. Rekepalli, K. Munch, M. Schierup, B. Lindow, W. C. Warren, D. Ray, R. E. Green, M. W. Bruford, X. Zhan, A. Dixon, S. Li, N. Li, Y. Huang, E. P. Derryberry, M. F. Bertelsen, F. H. Sheldon, R. T. Brumfield, C. V. Mello, P. V. Lovell, M. Wirthlin, M. P. C. Schneider, F. Prosdocimi, J. A. Samaniego, A. M. V. Velazquez, A. Alfaro-Núñez, P. F. Campos, B. Petersen, T. Sicheritz-Ponten, A. Pas, T. Bailey, P. Scofield, M. Bunce, D. M. Lambert, Q. Zhou, P. Perelman, A. C. Driskell, B. Shapiro, Z. Xiong, Y. Zeng, S. Liu, Z. Li, B. Liu, K. Wu, J. Xiao, X. Yinqi, Q. Zheng, Y. Zhang, H. Yang, J. Wang, L. Smeds, F. E. Rheindt, M. Braun, J. Fjeldsa, L. Orlando, F. K. Barker, K. A. Jønsson, W. Johnson, K.-P. Koepfli, S. O'Brien, D. Haussler, O. A. Ryder, C. Rahbek, E. Willerslev, G. R. Graves, T. C. Glenn, J. McCormack, D. Burt, H. Ellegren, P. Alström, S. V. Edwards, A. Stamatakis, D. P. Mindell, J. Cracraft, E. L. Braun, T. Warnow, W. Jun, M. T. P. Gilbert and G. Zhang. 2014. Whole-genome analyses resolve early branches in the tree of life of modern birds. Science 346:1320-1331.

Jones, M. E. H. 2008. Skull shape and feeding strategy in *Sphenodon* and other Rhynchocephalia. J. Morphol. 269:945-966.

Jønsson, K. A., P. H. Fabre, S. A. Fritz, R. S. Etienne, R. E. Ricklefs, T. B. Jørgensen, J. Fjeldså, C. Rahbek, P. G. P. Ericson, F. Woog, E. Pasquet, and M. Irestedt. 2012. Ecological and evolutionary determinants for the adaptive radiation of the Madagascan vangas. PNAS 109:6620-6625.

Kaiser, H., V. L. Carvalho, J. Ceballos, P. Freed, S. Heacox, B. Lester, S. J. Richards, C. R. Trainor, C. Sanchez, and M. O'Shea. 2011. The herpetofauna of Timor-Leste: a first report. ZooKeys 109:19-86.

Keogh, J.S. 1998. Molecular phylogeny of elapid snakes and a consideration of their biogeographic history. Biol J Linnean Soc 63:177-203.

Kimmel, C. B., B. Sidlauskas, and J. A. Clack. 2009. Linked morphological changes during palate evolution in early tetrapods. J Anat 215:91-109.

Klingenberg, C. P. 1996. Multivariate allometry. Pp. 23-49 *in* L. F. Marcus, M. Corti, A. Loy, G. J. P. Naylor, and D. E. Slice, eds. Advances in morphometrics. Springer US, Boston.

Klingenberg, C. P. 2010. Evolution and development of shape: integrating quantitative approaches. Nat Rev Genet 11:623-635.

Klingenberg, C. P. 2016. Size, shape, and form: concepts of allometry in geometric morphometrics. Dev Genes Evol 226:1-25.

Klingenberg, C. P., M. Barluenga, and A. Meyer. 2002. Shape analysis of symmetric structures: quantifying variation among individuals and asymmetry. Evolution 56:1909-1920.

Kohlsdorf, T., M. B. Grizante, C. A. Navas, and A. Herrel. 2008. Head shape evolution in Tropidurinae lizards: does locomotion constrain diet? J Evol Biol 21:781-790.

Lappin, A. K., and M. E. H. Jones 2014. Reliable quantification of bite-force performance requires use of appropriate biting substrate and standardization of bite out-lever. J Exp Biol 217:4303-4312.

Losos, J. B. 2011. Convergence, adaptation, and constraint. Evolution 65:1827-1840.

Losos, J. B. 1990. Ecomorphology, performance capability, and scaling of west Indian *Anolis* lizards: an evolutionary analysis. Ecol Monogr 60:369-388.

Losos, J. B. and D. L. Mahler. 2010. Adaptive radiation: the interaction of ecological opportunity, adaptation, and speciation. Pp. 381-420 *in* M. A. Bell, D. J. Futuyma, W. F. Eanes, and J. S. Levinton, eds. Evolution since Darwin: the first 150 years. Sinauer Association, Sunderland.

Losos, J. B. and R. E. Ricklefs. 2009. Adaptation and diversification on islands. Nature 457:830-836.

Lovette, I. J., E. Bermingham, and R. E. Ricklefs. 2002. Clade-specific morphological diversification and adaptive radiation in Hawaiian songbirds. Proc. R. Soc. B. 269:37-42.

Maddison, W. P. and D. R. Maddison. 2018. Mesquite: a modular system for evolutionary analysis. http://mesquiteproject.org.

Melville, J., E. G. Ritchie, S. N. J. Chapple, R. E. Glor, and J. A. Schulte. 2011. Evolutionary origins and diversification of dragon lizards in Australia's tropical savannas. Mol Phylogenet Evol 58:257-270.

Melville, J., J. A. Schulte, and A. Larson. 2001. A molecular phylogenetic study of ecological diversification in the Australian lizard genus *Ctenophorus*. J Exp Zool 291:339-353.

Melville, J., K. Smith, R. Hobson, S. Hunjan, and L. Shoo. 2014. The role of integrative taxonomy in the conservation management of cryptic species: the taxonomic status of endangered earless dragons (Agamidae: *Tympanocryptis*) in the grasslands of Queensland, Australia. PLOS ONE 9:e101847.

Monteiro, L. R. and M. R. Nogueira. 2010. Adaptive radiation, ecological specialisation, and the evolutionary integration of complex morphological structures. Evolution 64:724-744.

Oliver, P. M. and A. F. Hugall. 2017. Phylogenetic evidence for mid-Cenozoic turnover of a diverse continental biota. Nat. Ecol. Evol. 1:1896.

Olson, E. C. 1961. Jaw mechanisms: rhipidistians, amphibians, reptiles. Amer Zool 1:205-215.

Osborn, H. F. 1902. The law of adaptive radiation. Am Nat 36:353-363.

Pianka, E. R. 1971. Ecology of the agamid lizard *Amphibolurus isolepis* in Western Australia. Copeia 1971:527-536.

Pianka, E. R. 2013a. Notes on the ecology and natural history of two uncommon arboreal agamid lizards *Diporiphora*. West Austral Nat 29:77-84.

Pianka, E. R. 2013b. Notes on the ecology and natural history of two uncommon terrestrial agamid lizards *Ctenophorus clayi* and *C. fordi* in the Great Victoria Desert of Western Australia. West Austral Nat 29:85-93.

Pianka, E. R. 2013c. Notes on the natural history of the rarely recorded agamid lizard *Caimanops amphiboluroides* in Western Australia. West Austral Nat 29:99-102.

Pianka, E. R. 2014. Notes on a collection of lizards from the Eucla sand dunes in Western Australia. West Austral Nat 30:155-161.

Pianka, E. R. and H. D. Pianka. 1970. The ecology of *Moloch horridus* (Lacertilia: Agamidae) in Western Australia. Copeia 1970:90-103.

Pierce, S. E., K. D. Angielczyk, and E. J. Rayfield. 2008. Patterns of morphospace occupation and mechanical performance in extant crocodilian skulls: a combined geometric morphometric and finite element modeling approach. J Morphol 269:840-864.

Popescu, A. A., K. T. Huber, and E. Paradis. 2012. ape 3.0: new tools for distance-based phylogenetics and evolutionary analysis in R. Bioinformatics 28:1536-1537.

Pyron, R. A., F. T. Burbrink, and J. J. Wiens. 2013. A phylogeny and revised classification of Squamata, including 4161 species of lizards and snakes. BMC Evol Biol 13:1-53.

R Core Team 2018. R: A language and environment for statistical computing. R foundation for Statistical Computing, Vienne, Austria. https://www.R-project.org/

Revell, L. J. 2012. phytools: an R package for phylogenetic comparative biology (and other things). Methods Ecol Evol 3:217-223.

Ricklefs, R. E. 2004. Cladogenesis and morphological diversification in passerine birds. Nature 430:338.

Sakamoto, M. and M. Ruta. 2012. Convergence and divergence in the evolution of cat skulls: temporal and spatial patterns of morphological diversity. PLOS ONE 7:e39752.

Sanders, K.L., Lee, M.S.Y., Leys, R., Foster, R., Keogh, J.S. 2008. Molecular phylogeny and divergence dates for Australasian elapids and sea snakes (Hydrophiinae): evidence from seven genes for rapid evolutionary radiations. J Evol Biol 21:682-695.

Sanger, T. J., D. L. Mahler, A. Abzhanov, and J. B. Losos. 2012. Roles for modularity and constraint in the evolution of cranial diversity among *Anolis* lizards. Evolution 66:1525-1542.

Schluter, D. 2000. The ecology of adaptive radiation. Oxford University Press, New York.

Sereno, P. C. 1999. Definitions in phylogenetic taxonomy: critique and rationale. Syst Biol 48:329-351.

Shine, R. 1990. Function and evolution of the frill of the frillneck lizard, *Chlamydosaurus kingii* (Sauria: Agamidae). Biol. J. Linnean Soc. 40:11-20.

Shoo, L., R. Rose, P. Doughty, J. J. Austin, and J. Melville. 2008. Diversification of pebble-mimic dragons are consistent with historical disruption of important corridors in arid Australia. Mol Phylogenetics Evol 48:528-542.

Sidlauskas, B. 2008. Continuous and arrested morphological diversification in sister clades of characiform fishes: a phylomorphospace approach. Evolution 62:3135-3156.

Skinner, A., Hugall, A.F., Hutchinson, M.N. 2011. Lygosomine phylogeny and the origins of Australian scincid lizards. J Biogeogr 38:1044-1058.

Skyscan. 2011. NRecon. Aartselaar, Belgium.

Somaweera, R. and N. Somaweera. 2009. Lizards of Sri Lanka: a colour guide with field keys, Andreas S. Brahm.

Stayton, C. T. 2011. Biomechanics on the half shell: functional performance influences patterns of morphological variation in the emydid turtle carapace. Zoology 114:213-223.

Stayton, C. T. 2015a. The definition, recognition, and interpretation of convergent evolution, and two new measures for quantifying and assessing the significance of convergence. Evolution 69:2140-2153.

Stayton. C. T. 2015b Package ‘convevol. Available at https:// cran.r-project.org/web/ packages/convevol/index.html.

Sturmbauer, C., U. Hainz, S. Baric, E. Verheyen, and W. Salzburger. 2003. Evolution of the tribe Tropheini from Lake Tanganyika: synchronized explosive speciation producing multiple evolutionary parallelism. Hydrobiologia 500:51-64.

Throckmorton, G. S., J. D. Bavay, W. Chaffey, B. Merrotsy, S. Noske, and R. Noske. 1985. The mechanism of frill erection in the bearded dragon *Amphibolurus barbatus* with comments on the jacky lizard *A. muricatus* (Agamidae). J Morphol 183:285-292.

Tokita, M., W. Yano, H. F. James, and A. Abzhanov. 2017. Cranial shape evolution in adaptive radiations of birds: comparative morphometrics of Darwin's finches and Hawaiian honeycreepers. Phil Trans R Soc B 372:20150481.

Vermeij, G. J. 1973. Adaptation, versatility, and evolution. Syst Biol 22:466-477.

Vidal, N., Marin, J., Sassi, J., Battistuzzi, F.U., Donnellan, S., Fitch, A.J., Fry, B.G., Vonk, F.J., Rodriguez de la Vega, R.C., Couloux, A., Hedges, S.B. 2012. Molecular evidence for an Asian origin of monitor lizards followed by Tertiary dispersals to Africa and Australasia. Biol Letters rsbl20120460.

Visualization Sciences Group. 2013. Avizo. FEI Corporate Headquarters, Oregon.

Watanabe, A. 2018. How many landmarks are enough to characterize shape and size variation? PLOS ONE 13:e0198341.

Wiley, D., N. Amenta, D. Alcantara, D. Ghosh, Y. Kil, and E. Delson. 2007. Landmark Editor: Institute for Data Analysis and Visualization. University of California, Davis.

Wilson, G. P., A. R. Evans, I. J. Corfe, P. D. Smits, M. Fortelius, and J. Jernvall. 2012. Adaptive radiation of multituberculate mammals before the extinction of dinosaurs. Nature 483:457-460.

Wilson, S. and G. Swan. 2013. A complete guide to reptiles of Australia. New Holland Publishers, Chatswood.

Zelditch, M. L., D. L. Swiderski, H. D. Sheets, and W. L. Fink. 2012. Geometric morphometrics for biologists: a primer, Academic Press.

Tables

Table 1 – Examining evolutionary allometry: the effect of cranium centroid size and ecological life habit on cranial shapes within the 52 sampled species of agamid as evaluated by a phylogenetic least squares model (shape ~ log (size) * life habit). Statistical significance was evaluated by permutation using 1000 iterations. Bold indicates significant *P*-values (less than 0.05).

	DF	SS	MS	R^2	F	Z	*P*-value
Log (size)	1	0.728	0.729	0.112	7.704	5.520	**0.001**
Life habit	3	1.073	0.358	0.165	3.782	5.462	**0.001**
Log (size) : life habit	3	0.543	0.181	0.084	1.916	4.960	**0.001**
Residuals	44	4.160	0.095	0.640			
Total	51	6.505					

Figure legends

Figure 1 – Consensus tree of the 52 agamid species studied here, with topology inferred from multiple sources of recent phylogenetic studies (Melville et al. 2001; Hugall et al. 2008; Shoo et al. 2008; Melville et al. 2011; Pyron et al. 2013; Melville et al. 2014), and branch lengths calculated using the Grafen (1989) computation method (which calculates branch lengths based

634 on number of operational taxonomic units). Coloured points to indicate life habits, and coloured
635 tree branches to show the five major monophyletic clades.
636
637 Figure 2 – Landmarks used to characterise cranial shape in 3D. Landmarks digitised on the
638 cranium surface in dorsal view (A), palatal view (B) lateral view (C), and posterior view (D).
639 Numbers are based on scheme used in IDAV Landmark Editor, and can be matched to
640 definitions in supplementary material: Table S5.2.
641
642 Figure 3 – Evolutionary allometry examined by a multivariate regression of shape on log-
643 transformed centroid size (A). In B, 3D triangular meshes representing the shape of the largest
644 and smallest sampled crania as predicted by the regression are shown, warped from an average-
645 shape mesh using thin-plate spline approach. From top to bottom: dorsal, lateral, ventral, and
646 occipital views.
647
648 Figure 4 – The major axes of variation in cranial shape (from a PCA of allometry-free shape
649 variables), depicted as warped cranial surfaces. Cranial shape differences associated with the first
650 four PCs are shown as 3D triangular meshes representing the shape at the positive and negative
651 end of each axis (PC score given), warped from an average-shape mesh using thin-plate spline
652 approach.
653
654 Figure 5 – Phylomorphospaces for PC1 versus PC2 (A), and PC3 versus PC4 (B), illustrating the
655 distribution of life habit groups in the allometry-free cranial morphospace. Points are coloured by

life habit (as given in legend). Cranium images are 3D triangular meshes of actual specimens that represent extremes of the shape variation, oriented in anterolateral view.

Figure 6 – Allometry-free cranial morphospaces of PC1 versus PC2 (A), and PC3 versus PC4 (B), with convex hulls mapped on to represent the disparity and morphospace occupation of the two core lineages of the Amphibolurinae, the *Amphibolurus* group and the *Ctenophorus* group.

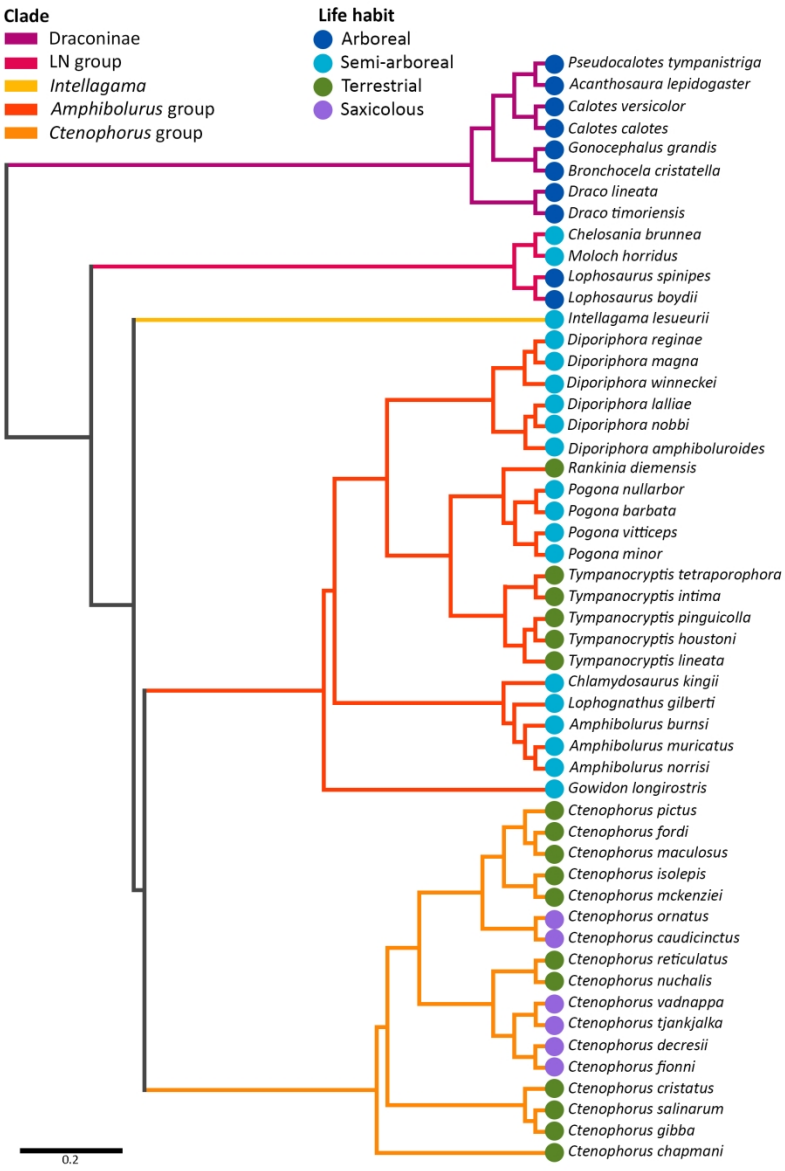

Figure 1 – Consensus tree of the 52 agamid species studied here, with topology inferred from multiple sources of recent phylogenetic studies (Melville et al. 2001; Hugall et al. 2008; Shoo et al. 2008; Melville et al. 2011; Pyron et al. 2013; Melville et al. 2014), and branch lengths calculated using the Grafen (1989) computation method (which calculates branch lengths based on number of operational taxonomic units). Coloured points to indicate life habits, and coloured tree branches to show the five major monophyletic clades.

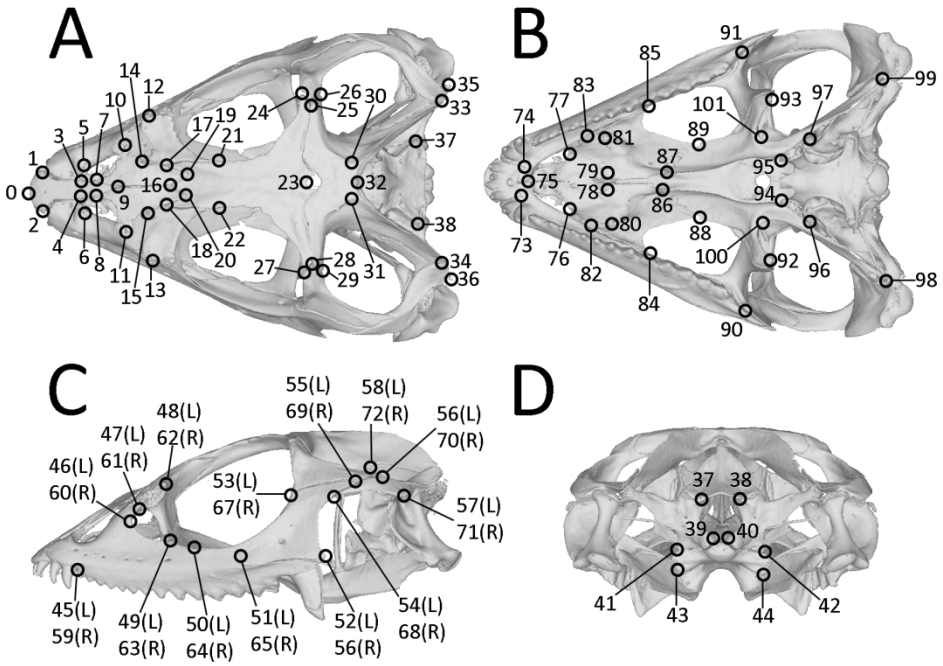

Figure 2 – Landmarks used to characterise cranial shape in 3D. Landmarks digitised on the cranium surface in dorsal view (A), palatal view (B) lateral view (C), and posterior view (D). Numbers are based on scheme used in IDAV Landmark Editor, and can be matched to definitions in supplementary material: Table S5.2.

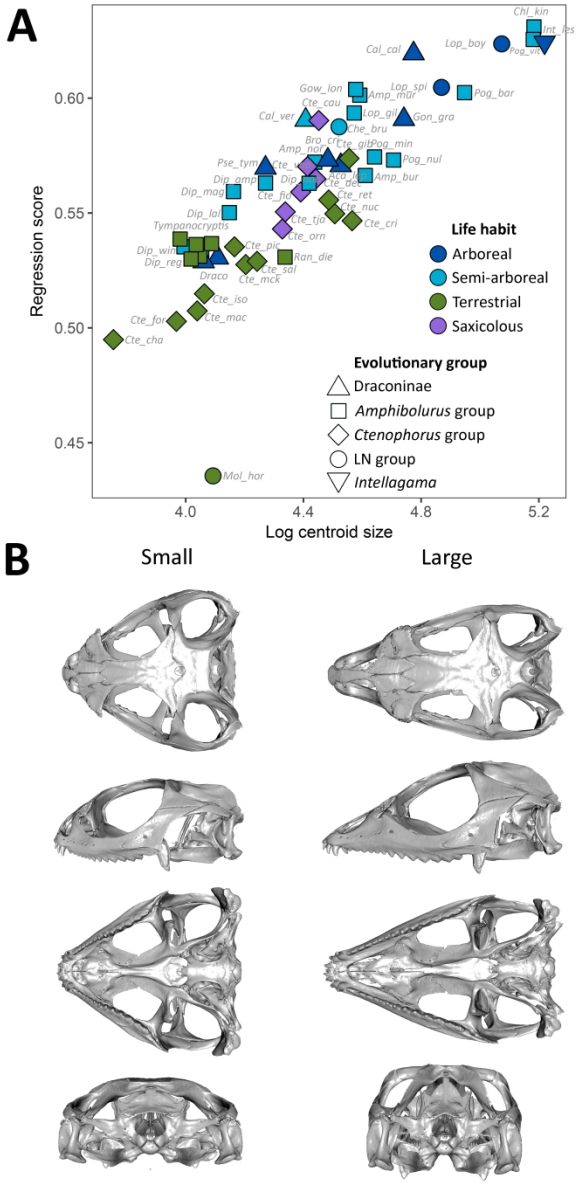

Figure 3 – Evolutionary allometry examined by a multivariate regression of shape on log-transformed centroid size (A). In B, 3D triangular meshes representing the shape of the largest and smallest sampled crania as predicted by the regression are shown, warped from an average-shape mesh using thin-plate spline approach. From top to bottom: dorsal, lateral, ventral, and occipital views.

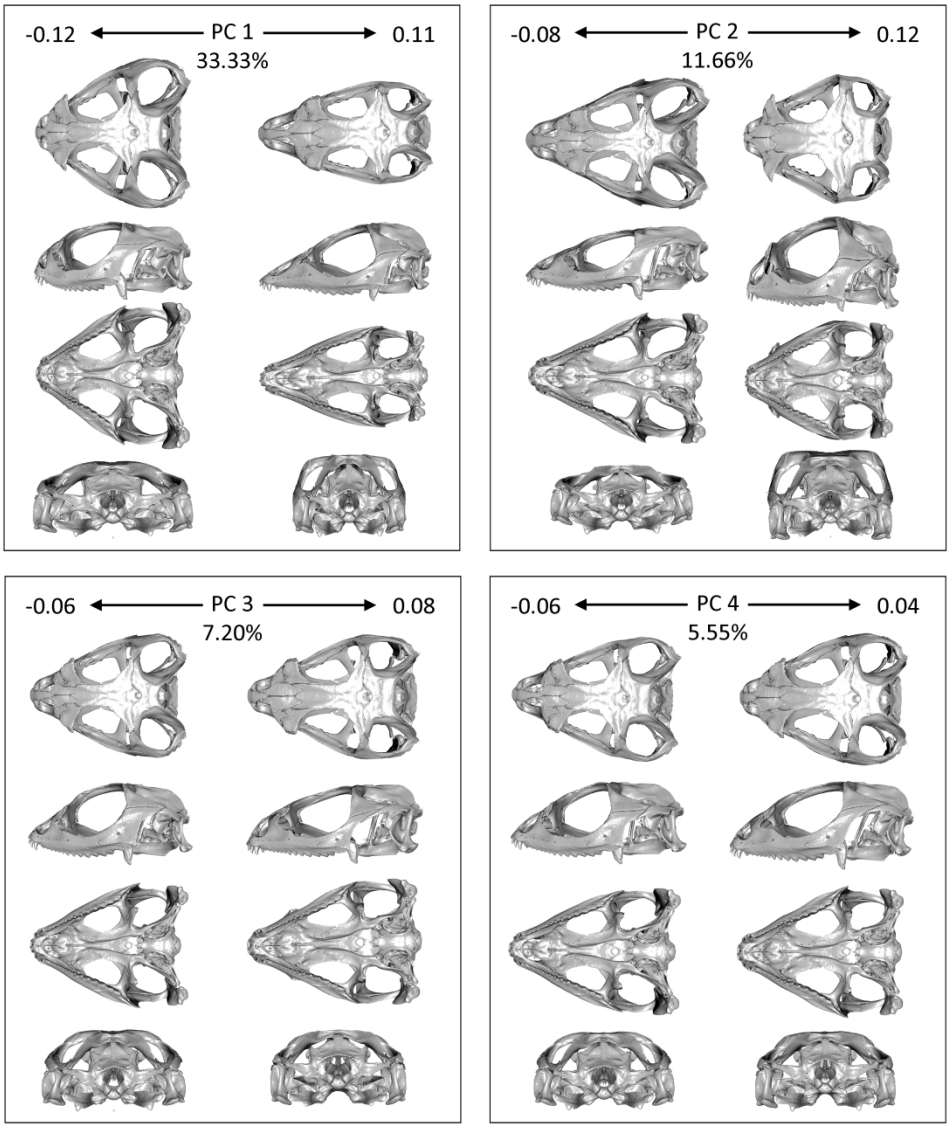

Figure 4 – The major axes of variation in cranial shape (from a PCA of allometry-free shape variables), depicted as warped cranial surfaces. Cranial shape differences associated with the first four PCs are shown as 3D triangular meshes representing the shape at the positive and negative end of each axis (PC score given), warped from an average-shape mesh using thin-plate spline approach.

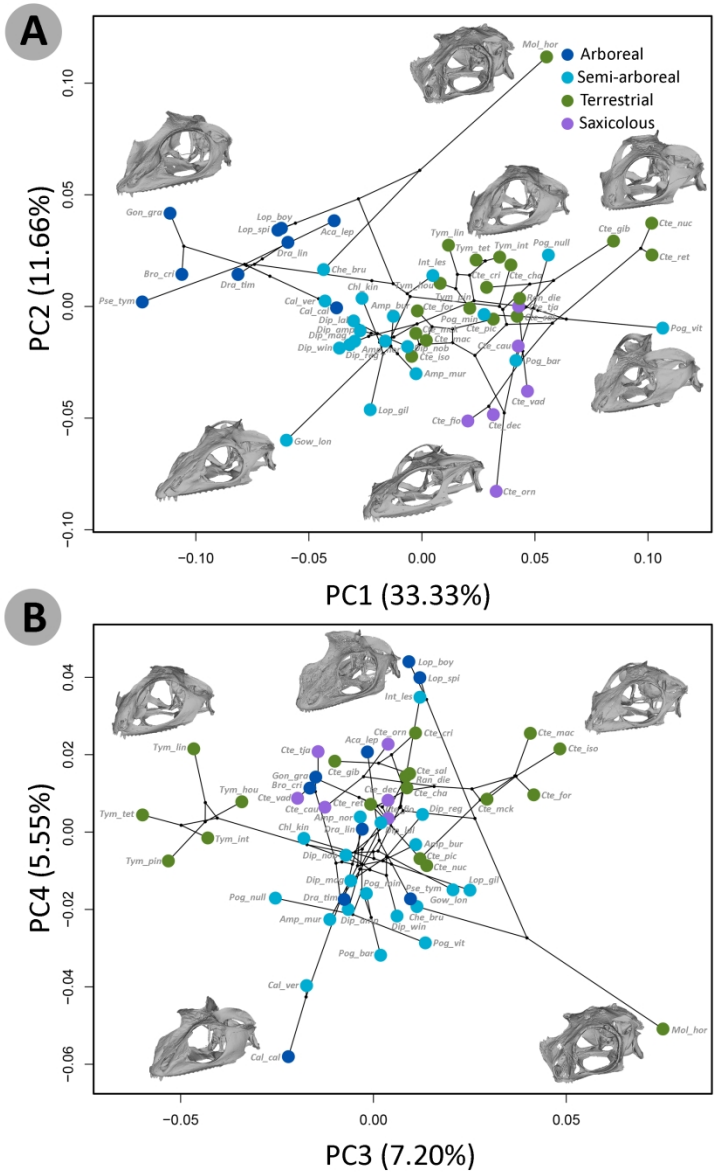

Figure 5 – Phylomorphospaces for PC1 versus PC2 (A), and PC3 versus PC4 (B), illustrating the distribution of life habit groups in the allometry-free cranial morphospace. Points are coloured by life habit (as given in legend). Cranium images are 3D triangular meshes of actual specimens that represent extremes of the shape variation, oriented in anterolateral view.

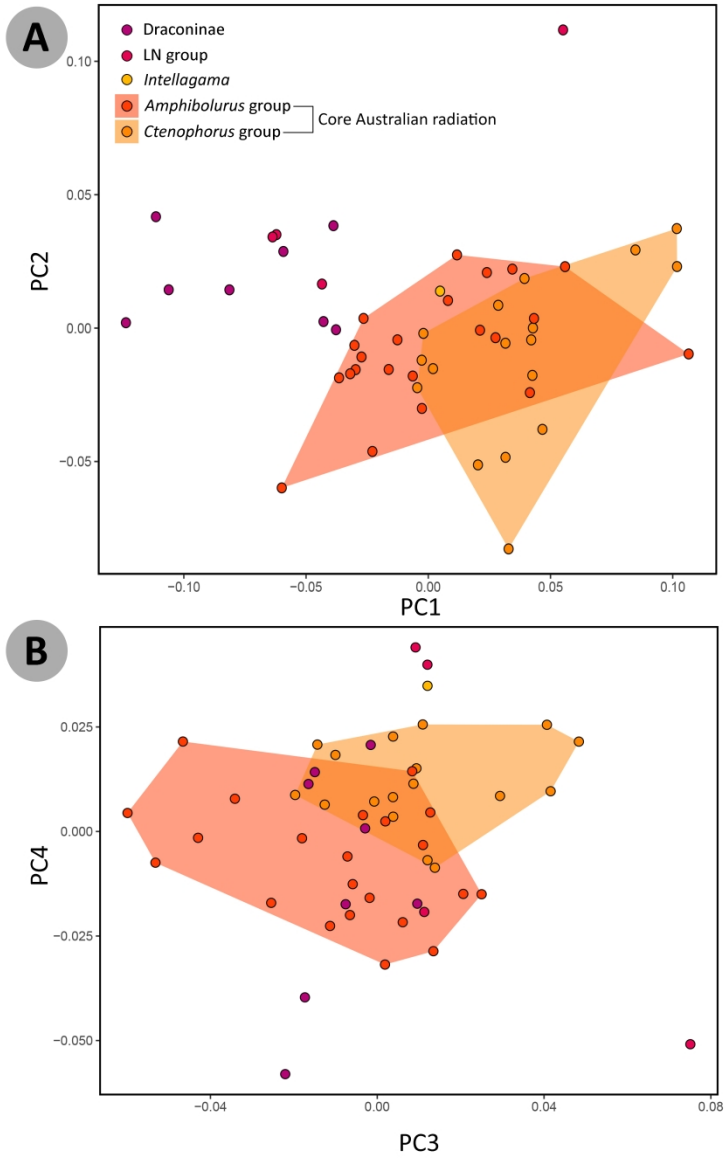

Figure 6 – Allometry-free cranial morphospaces of PC1 versus PC2 (A), and PC3 versus PC4 (B), with convex hulls mapped on to represent the disparity and morphospace occupation of the two core lineages of the Amphibolurinae, the Amphibolurus group and the Ctenophorus group.

Table S1 – Specimens used in shape analyses and relevant information. SAMA = South Australian Museum; AMS = Australian Museum. LN = Least nested group.

Genus	Species	Evolutionary Group	Reg. number	Specimen	Life habit
Acanthosaura	*lepidogaster*	Draconinae	SAMA R64182	Head	Arboreal
Amphibolurus	*burnsi*	*Amphibolurus*	SAMA R30986	Head	Semi-arboreal
Amphibolurus	*muricatus*	*Amphibolurus*	AMS R154972	Head	Semi-arboreal
Amphibolurus	*norrisi*	*Amphibolurus*	SAMA R60767	Head	Semi-arboreal
Bronchocela	*cristatella*	Draconinae	SAMA R22477	Skull	Arboreal
Calotes	*calotes*	Draconinae	SAMA R47735	Skull	Arboreal
Calotes	*versicolor*	Draconinae	SAMA R66808	Skull	Semi-arboreal
Chelosania	*brunnea*	LN	SAMA R140288	Head	Semi-arboreal
Chlamydosaurus	*kingii*	*Amphibolurus*	SAMA R21373	Skull	Semi-arboreal
Ctenophorus	*caudicinctus*	*Ctenophorus*	SAMA R61888	Head	Saxicolous
Ctenophorus	*chapmani*	*Ctenophorus*	SAMA R59616	Head	Terrestrial
Ctenophorus	*cristatus*	*Ctenophorus*	SAMA R59493	Head	Terrestrial
Ctenophorus	*decresii*	*Ctenophorus*	SAMA R53234	Skull	Saxicolous
Ctenophorus	*fionni*	*Ctenophorus*	SAMA R68126	Head	Saxicolous
Ctenophorus	*fordi*	*Ctenophorus*	SAMA R34489	Head	Terrestrial
Ctenophorus	*gibba*	*Ctenophorus*	SAMA R43604	Head	Terrestrial
Ctenophorus	*isolepis*	*Ctenophorus*	SAMA R59391	Head	Terrestrial
Ctenophorus	*maculatus*	*Ctenophorus*	SAMA R59600	Head	Terrestrial
Ctenophorus	*mckenziei*	*Ctenophorus*	SAMA R26160	Head	Terrestrial
Ctenophorus	*nuchalis*	*Ctenophorus*	SAMA R7296	Skull	Terrestrial
Ctenophorus	*ornatus*	*Ctenophorus*	SAMA R56064	Head	Saxicolous
Ctenophorus	*pictus*	*Ctenophorus*	SAMA R28608	Head	Terrestrial
Ctenophorus	*reticulatus*	*Ctenophorus*	SAMA R46987	Head	Terrestrial
Ctenophorus	*salinarum*	*Ctenophorus*	SAMA R59079	Head	Terrestrial
Ctenophorus	*tjankjalka*	*Ctenophorus*	SAMA R53804	head	Saxicolous
Ctenophorus	*vadnappa*	*Ctenophorus*	SAMA R45802	Head	Saxicolous
Diporiphora	*amphiboluroides*	*Amphibolurus*	SAMA R4838C	Head	Semi-arboreal
Diporiphora	*lalliae*	*Amphibolurus*	SAMA R65868	Head	Semi-arboreal
Diporiphora	*magna*	*Amphibolurus*	SAMA R58365	Head	Semi-arboreal
Diporiphora	*nobbi*	*Amphibolurus*	SAMA R21511	Head	Semi-arboreal
Diporiphora	*reginae*	*Amphibolurus*	SAMA R63999	Head	Semi-arboreal
Diporiphora	*winneckei*	*Amphibolurus*	SAMA R66514	Head	Semi-arboreal
Draco	*lineatus*	Draconinae	AMS R57460	Head	Arboreal
Draco	*timoriensis*	Draconinae	SAMA R13860B	Head	Arboreal
Gonocephalus	*grandis*	Draconinae	SAMA R66697	Skull	Arboreal
Gowidon	*longirostris*	*Amphibolurus*	SAMA R18053	Skull	Semi-arboreal
Intellagama	*lesueurii*	*Intellagama*	SAMA R27305	Skull	Semi-arboreal
Lophosaurus	*boydii*	LN	AMS R68782	Head	Arboreal
Lophognathus	*gilberti*	*Amphibolurus*	SAMA R38793	Head	Semi-arboreal
Lophosaurus	*spinipes*	LN	SAMA R40742	Head	Arboreal
Moloch	*horridus*	LN	SAMA R17325	Head	Terrestrial
Pogona	*barbata*	*Amphibolurus*	SAMA R32503	Head	Semi-arboreal
Pogona	*minor*	*Amphibolurus*	SAMA R36706	Skull	Semi-arboreal
Pogona	*nullarbor*	*Amphibolurus*	SAMA R18581	Skull	Semi-arboreal
Pogona	*vitticeps*	*Amphibolurus*	SAMA R18545	Skull	Semi-arboreal
Pseudocalotes	*tympanistriga*	Draconinae	SAMA R35730	Head	Arboreal
Rankinia	*diemensis*	*Amphibolurus*	SAMA R1457B	Head	Terrestrial
Tympanocryptis	*houstoni*	*Amphibolurus*	SAMA R63157	Head	Terrestrial
Tympanocryptis	*intima*	*Amphibolurus*	SAMA R51044	Head	Terrestrial
Tympanocryptis	*lineata*	*Amphibolurus*	SAMA R59721	Head	Terrestrial
Tympanocryptis	*pinguicolla*	*Amphibolurus*	SAMA R44672	Head	Terrestrial
Tympanocryptis	*tetraporophora*	*Amphibolurus*	SAMA R67710	Head	Terrestrial

Table S2 – Landmark definitions for landmarks used to characterise 3D cranial shape. Numbers correspond to format used in IDAV Landmark Editor (starting at 0). See Evans 2008 for nomenclature of structures. R = right, L = left, B = both/between.

Number	Bone	Description
0	Premaxilla	Most anterior tip of the premaxilla (snout)
1	Premaxilla (R)	Most lateral external point along the alveolar margin.
2	Premaxilla (L)	Most lateral external point along the alveolar margin.
3	Maxilla (R)	Most dorsomedial external point of the maxilla-premaxilla process
4	Maxilla (L)	Most dorsomedial external point of the maxilla-premaxilla process
5	Maxilla (R)	Most anterior external point of the anterior of narial basin foramen
6	Maxilla (L)	Most anterior external point of the anterior of narial basin foramen
7	Nasal (R)	Anterior-most point along the lateral margin (external)
8	Nasal (L)	Anterior-most point along the lateral margin (external)
9	Premaxilla	Most posterodorsal tip (external)
10	Nasal (R)	Most anterior point of nasal-maxilla suture seam (external)
11	Nasal (L)	Most anterior point of nasal-maxilla suture seam (external)
12	Maxilla (R)	Most posterodorsal point of lateral facial process
13	Maxilla (L)	Most posterodorsal point of lateral facial process
14	Prefrontal (R)	Most anteromedial point of prefrontal-nasal process
15	Prefrontal (L)	Most anteromedial point of prefrontal-nasal process
16	Frontal	Most anterior point along the midline
17	Frontal	Most anterolateral point, (right) near the junction of the nasal-maxillary-prefrontal suture seams
18	Frontal	Most anterolateral point, (left) near the junction of the nasal-maxillary-prefrontal suture seams
19	Nasal (R)	Most posterior point externally visible
20	Nasal (L)	Most posterior point externally visible
21	Frontal	Most posterior point (right) of prefrontal-frontal suture seam (along the orbital margin)
22	Frontal	Most posterior point (right) of prefrontal-frontal suture seam (along the orbital margin)
23	Frontal	Posteromedial point of frontal (anterior of parietal foramen)
24	Frontal	Most lateral point along the orbital margin
25	Postorbital (R)	Most dorsal external point
26	Parietal	Most lateral point of right postorbital-parietal suture, along the edge of the upper temporal fenestra
27	Frontal	Most posterolateral point, near the junction of the frontal-postfrontal-parietal suture seam
28	Postorbital (L)	Most dorsal external point
29	Parietal	Most lateral point of left postorbital-parietal suture, along the edge of the upper temporal fenestra
30	Parietal	Most medial point of the right side of the parietal platform (or centre of the most medial point where it is long)
31	Parietal	Most medial point of the left side of the parietal platform (or centre of the most medial point where it is long)
32	Parietal	Most posterior point of the parietal platform (middle)
33	Squamosal (R)	Most posterodorsal point
34	Squamosal (L)	Most posterodorsal point
35	Supratemporal (R)	Most posterior point
36	Supratemporal (L)	Most posterior point

37	Supraoccipital	Most posterior point of the right external supraoccipital-otooccipital suture
38	Supraoccipital	Most posterior point of the left external supraoccipital-otooccipital suture
39	Otooccipital (L)	Most medial point along the foramen magnum
40	Otooccipital (R)	Most medial point along the foramen magnum
41	Basioccipital	Most posterodorsal point of the basal tubercle, near where it meets the otooccipital (left)
42	Basioccipital	Most posterodorsal point of the basal tubercle, near where it meets the otooccipital (right)
43	Basioccipital	Most ventral point of the side of the basal tubercle (left)
44	Basioccipital	Most ventral point of the side of the basal tubercle (right)
45	Maxilla (L)	Most posterior point of the most posterior pleurodont tooth attachment
46	Maxilla (L)	Most anterior point of the lacrimal opening
47	Prefrontal (L)	Most posterior point of the lateral enlargement (meets with maxilla)
48	Prefrontal (L)	Posteromedial limit of the prefrontal lateral enlargement
49	Maxilla (L)	Point along the orbital margin near the junction of the maxilla-prefrontal-palatal suture seams
50	Maxilla (L)	Point along the orbital margin level with most anterior external part of jugal
51	Maxilla (L)	Most posterior point of the posterodorsal process (along the boundary with the jugal)
52	Jugal(L)	Most posteroventral point
53	Postorbital (L)	Most anteroventral external point
54	Squamosal (L)	Most posterior external point
55	Jugal (L)	Most posterior external point
56	Postorbital (L)	Most posterior point
57	Squamosal (L)	Most posteroventral (often broadest) point of the "ventral peg" (see Evans 2008)
58	Supratemporal (L)	Most anterior point along the margin of upper temporal fenestra
59	Maxilla (R)	Most posterior point of the most posterior pleurodont tooth attachment
60	Maxilla (R)	Most anterior point of the lacrimal opening
61	Prefrontal (R)	Most posterior point of the lateral enlargement (meets with maxilla)
62	Prefrontal (R)	Posteromedial limit of the prefrontal lateral enlargement
63	Maxilla (R)	Point along the orbital margin near the junction of the maxilla-prefrontal-palatal suture seams
64	Maxilla (R)	Point along the orbital margin level with most anterior external part of jugal
65	Maxilla (R)	Most posterior point of the posterodorsal process (along the boundary with the jugal)
66	Jugal(R)	Most posteroventral point
67	Postorbital (R)	Most anteroventral external point
68	Squamosal (R)	Most posterior external point
69	Jugal (R)	Most posterior external point
70	Postorbital (R)	Most posterior point
71	Squamosal (R)	Most posteroventral (often broadest) point of the "ventral peg" (see Evans 2008)
72	Supratemporal (R)	Most anterior point along the margin of upper temporal fenestra
73	Premaxilla	Most posteroventral point (right)
74	Premaxilla	Most posteroventral point (left)
75	Maxilla (B)	Most posterior point of the join in the maxillary lappet along the midline (see Evans 2008)
76	Vomer (R)	Most posterolateral point where it meets the palatine
77	Vomer (L)	Most posterolateral point where it meets the palatine
78	Vomer (R)	Most posterior point

79	Vomer (L)	Most posterior point
80	Palatine (R)	Most anterolateral point of the medial flange
81	Palatine (L)	Most anterolateral point of the medial flange
82	Palatine (R)	Most anterior point of the external maxillary-palatine suture seam
83	Palatine (L)	Most anterior point of the external maxillary-palatine suture seam
84	Palatine (R)	Most posterior point of the external maxillary-palatine suture seam
85	Palatine (L)	Most posterior point of the external maxillary-palatine suture seam
86	Palatine (R)	Most anterior point of palatine-pterygoid suture seam (ventral)
87	Palatine (L)	Most anterior point of palatine-pterygoid suture seam (ventral)
88	Pterygoid (R)	Most posterior point of palatine-pterygoid suture seam (ventral)
89	Pterygoid (L)	Most posterior point of palatine-pterygoid suture seam (ventral)
90	Maxilla (R)	Posterior limit of tooth row (level with an enlargement of the jugal)
91	Maxilla (L)	Posterior limit of tooth row (level with an enlargement of the jugal)
92	Pterygoid (R)	Most ventral point of pterygoid process
93	Pterygoid (L)	Most ventral point of pterygoid process
94	Basipterygoid	Most anterior point of right basipterygoid process
95	Basipterygoid	Most anterior point of left basipterygoid process
96	Basipterygoid	Most posterior point of right basipterygoid process
97	Basipterygoid	Most posterior point of left basipterygoid process
98	Pterygoid (R)	Most posteroventral point (closest to quadrate)
99	Pterygoid (L)	Most posteroventral point (closest to quadrate)
100	Pterygoid (R)	Most medial point of posterolateral edge (medial to pterygoid flange)
101	Pterygoid (L)	Most medial point of posterolateral edge (medial to pterygoid flange)

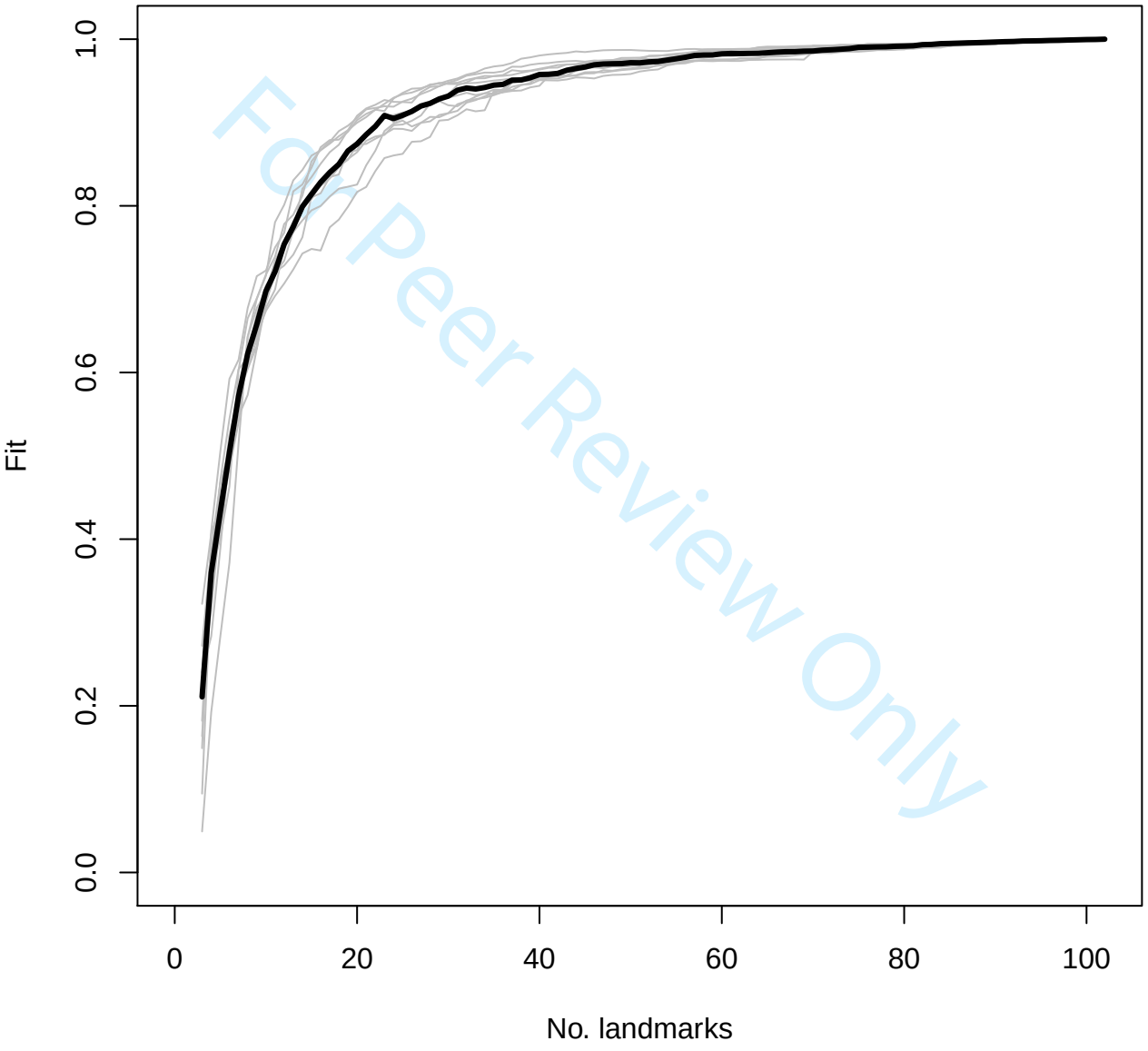

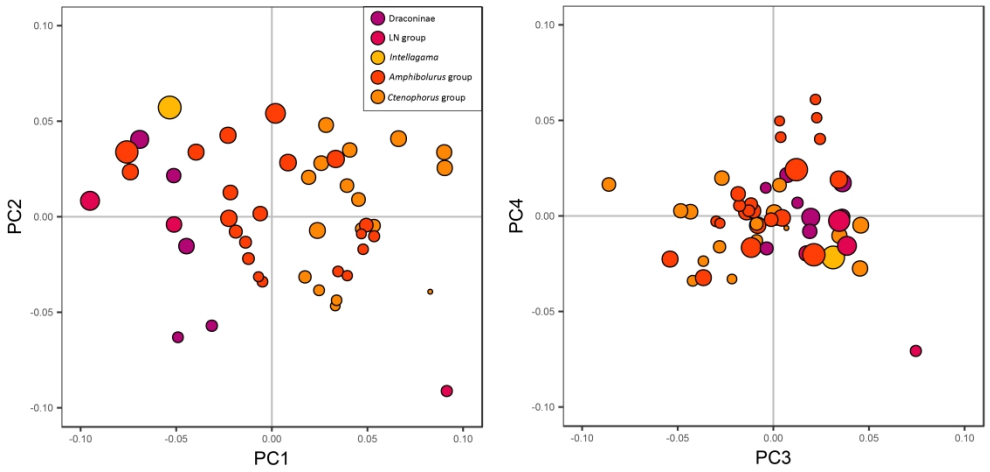

Appendix 4 - Figure S2 - PCA before allometry correction

Appendix 4 – Summary for first six principal components, for principal components analysis of allometry corrected shape variables.

	PC 1	PC 2	PC 3	PC 4	PC 5	PC 6
Proportion of variance	0.333	0.117	0.072	0.056	0.048	0.044
Cumulative proportion	0.333	0.450	0.051	0.578	0.625	0.669